IEEE Access
Multidisciplinary | Rapid Review | Open Access Journal

Received 25 August 2025, accepted 24 September 2025, date of publication 26 September 2025, date of current version 2 October 2025.

Digital Object Identifier 10.1109/ACCESS.2025.3615074

RESEARCH ARTICLE

Hybrid RFID-GNSS Circuit for Robust Vehicular Navigation in Signal-Degraded Environments

PIERLUIGI ROSSI[1], (Member, IEEE), LUCA CATARINUCCI[2], (Senior Member, IEEE), MASSIMO CECCHINI[1], (Senior Member, IEEE), GIUSEPPE GRASSI[2], (Senior Member, IEEE), AND RICCARDO COLELLA[2], (Senior Member, IEEE)

[1]Department of Agriculture and Forest Sciences (DAFNE), Tuscia University, 01100 Viterbo, Italy
[2]Department of Innovation Engineering, University of Salento, 73100 Lecce, Italy

Corresponding authors: Riccardo Colella (riccardo.colella@unisalento.it) and Pierluigi Rossi (pierluigi.rossi@unitus.it)

This work was supported in part by the "Rome Technopole" Project, which is part of the Next Generation European Union (EU) Program, Italian's "Piano Nazionale di Ripresa e Resilienza (PNRR)," Mission 4, Component 2, Investment no. 1.5 under Grant ECS 0000024; and in part by the Project Tools for Electric Recharging Vehicle (TER), under Grant MIMIT CUP: B89J25001580005.

ABSTRACT This work presents the design and implementation of a novel hybrid GNSS–RFID circuit architecture aimed at enhancing positioning accuracy in environments where satellite navigation performance is degraded by signal obstruction and multipath effects. The RFID subsystem enhances global GNSS positioning by leveraging a network of local passive resonant circuits, i.e., UHF RFID tags, which act as local anchors. These RFID tags provide position refinement information that is used by the control circuit to improve localization performance. The theoretical model and the circuit-level implementation for the adaptive and dynamic power control over the RFID interface are presented, enabling the estimation of distance from local tags based on backscattered signal strength and controlled RF excitation levels. The circuit provides RFID-assisted dynamic reconfiguration of GNSS receiver parameters, including carrier-to-noise ratio thresholds (CN0), satellite angle-of-arrival filtering, and elevation-based 2D/3D mode switching. To validate the proposed circuit, experimental tests were conducted in three obstructed agricultural and forestry environments using U-blox Zed-F9P GNSS modules as the hardware platform. Positioning performance was compared between a standalone GNSS configuration and the same module augmented with the RFID-assisted circuit. A third Zed-F9P receiver, operating in real-time kinematic (RTK) fix mode, served as a ground-truth reference for accuracy evaluation. Positioning errors were evaluated using metrics such as mean error, median error, and error variance. Results demonstrate that the RFID-assisted architecture enables up to 43% reduction in positioning error and a significant decrease in error variance, confirming the robustness and adaptability of the proposed circuit under challenging conditions.

INDEX TERMS Navigation circuits and systems, GNSS, RFID, Zed-F9P, sensor-fusion.

I. INTRODUCTION

Real-time position assessment of vehicles through Global Navigation Satellite Systems (GNSS) is affected by several factors that degrade the overall precision, such as the presence of buildings, vegetation, terrain slope, and any other surrounding obstacles or specific conditions. Challenging environments, in fact, significantly influence the determination of ranges between spatial vehicles (satellites) and ground vehicles, leading to inaccuracies that add up to the receiver's clock error.

To overcome these issues, integrating GNSS with complementary technologies has become an essential strategy to significantly enhance accuracy or, at least, mitigate abnormal position readings to an acceptable level determined by the operational tasks and their precision requirements. A recent review of positioning methods tailored for agricultural and forestry contexts highlighted a wide array of technologies

The associate editor coordinating the review of this manuscript and approving it for publication was Arun Prakash.

and networks, recommending a hierarchical approach that optimally leverages sensor fusion and radio frequency identification (RFID) technologies, including both passive and active RFID tags [1]. However, integration methods aiming to process GNSS raw data with the help of additional information coming from RFID technologies have only explored the possibility of solving issues related to lack of GNSS data or limiting some of its downsides without, however, proposing circuit integration or data interoperability for finer tuning.

Several possibilities have emerged in this field of research, since recent advances in Ultra-Wide Band (UWB) technologies have shown significant potential through methods such as creating differential range measurement stations to estimate anchor biases [2] and employing multisensory fusion that combines GNSS with UWB data to enhance positioning accuracy significantly, especially in GNSS-challenged environments such as dense vegetation or urban structures [3]. RFID-only localization methods have also been tested in multiple environments and even as a stand-alone tool [4], [5], [6] especially in indoor environments [7], [8]. However, outdoor deployment of such methods encounters considerable challenges due to varying atmospheric conditions, soil moisture, humidity levels, and physical obstructions. Moreover, the use of 5G data, which has been explored in previous research [9], [10], cannot at the moment be considered a reliable mobile connection network in rural areas and should be therefore considered only after careful assessments of specific working areas. Despite these environmental limitations, combining RFID with GNSS has yielded notable improvements, particularly through filtering abnormal RFID tag readings and the detection of GNSS positional outliers [11]. RFID tags have shown considerable success when employed in combination with GNSS through triangulation techniques, leading to enhanced accuracy in complex operational environments [12], but in such cases there was no interaction among the two positioning algorithms.

Early multimodal platforms have shown that even simple passive-RFID grids can complement satellite and Wi-Fi signals: research has already explored a sensor fusion of GPS, Wi-Fi and UHF RFID on a grid-based Bayesian in a mixed indoor-outdoor area but did not exploit RFID data to improve raw GNSS observations [13]. Recent studies have begun to couple RFID with satellite or inertial positioning in very specific application domains, providing useful insights for a circuit-level hybrid approach: previous prototypes involved passive UHF tags embedded along a roadside are read by an on-board unit to refine GPS navigation for autonomous vehicles, demonstrating that tag-triggered map-matching can offset GNSS multipath at a negligible cost [14], and this is probably the most significant attempt to integrate such two technologies, with the utter advantage of exploiting passive tags.

Other solutions, instead, have been limited to specific sectors only, like agricultural mechanized farming tasks [15], introducing yield-mapping system based on a long-range RFID reader and a GNSS receiver positioned on a tractor with the only purpose of georeferencing and tagging each harvested bin without covering positioning or navigation enhanced capabilities. A similar application is represented by the use of RFID and GNSS for pasture-mowing operations [16], but again with active RFID tags. Additionally, RFID alone has proven valuable in precision agriculture contexts, notably in detecting vineyard and orchard rows, thereby directly facilitating precision agricultural operations such as targeted spraying [17].

One of the typical reasons for integrating such technologies is also given by the need of overcoming GNSS-denied environments, like tunnels [18], but since in such cases the system can only rely on RFID data or vice-versa, there was little space for them to work altogether and each system covered the downsides of the other without never being able to exploit them at the same time. Advances have been made, instead, on the integration of GNSS and UHF RFID antennas [19], with a dual-purpose L1-GPS/RFID reader backed by an artificial magnetic conductor surface.

This tendency of exploiting RFID to overcome GNSS limitations in indoor environments has also been tested in enterprise logistics architectures, fusing RFID tag readings with GNSS data in a middleware that enables track-and-trace of assets in warehouses and long-haul transport [20].

The combination of GNSS L1 receivers and UHF RFID readers have been explored for a low-cost cooperative localization method [11] which, however, does not support any direct interaction with raw GNSS data; in other cases, instead, active UHF RFID trilateration and RSSI-fingerprinting for pedestrian navigation was investigated, but it wasn't matched with GNSS receivers [21]. Studies have also extensively evaluated the effects of tuning the most critical GNSS parameters on receivers including Signal to Noise Ratio (SNR), Carrier to Noise Density Ratio (C/N0), geometric dilution of precision (GDOP), and zenith tropospheric delay (ZTD), highlighting their key role in determining positional accuracy, particularly in environments with dense vegetation [22], [23], [24]. These promising approaches also avoid operating on the final GNSS positioning solution, since they rather allow better quality on raw data acquisition right before obtaining any assessment from the receiver. Significant experimental efforts in this field involved the U-Blox ZED-F9P GNSS-RTK receiver, widely recognized for its operational flexibility [25], compatibility with multiple satellite constellations, customization capabilities and robust performance in challenging environmental conditions [26]. Research provided essential insights regarding the limits of precision attainable in densely obstructed environments, such as forested areas, which demonstrated substantial positional inaccuracies in GNSS measurements [27], [28], [29].

Given the current state of the art, this paper addresses critical gaps in sensor fusion technologies for GNSS receivers by introducing a novel hybrid RFID–GNSS circuit architecture, specifically designed to enhance positioning performance

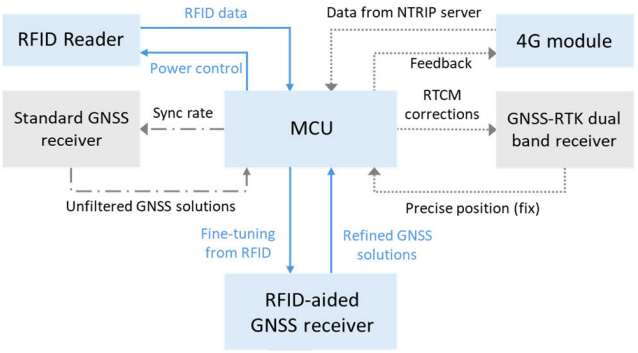

FIGURE 1. Circuit architecture and interconnections. Supplementary sub-circuits are shown in grey.

in environments where satellite signals are degraded by obstructions and multipath effects. The main contribution of this work lies in the definition of a new systems architecture providing the circuit-level combination of a UHF RFID high-frequency circuit interface with GNSS signal processing circuits, enabling the receiver to adapt its operating parameters in response to spatially distributed, passive RFID tags. Each RFID tag acts as a passive resonant circuit placed at known georeferenced positions in the environment, effectively serving as a local anchor that can support fine-grained positioning refinement. Upon detection of a tag, the circuit extracts tag-specific configuration data that can be used to dynamically reconfigure GNSS receiver parameters—such as carrier-to-noise ratio thresholds, angle-of-arrival limits, and 2D/3D mode selection— which have been previously configured according to the local context when the tag was georeferenced: the role of tags, in fact, is to carry an information that is related to the quality of GNSS signals that can be received from their position, which can be assessed by looking at signal degradation during georeferencing activities and by considering filed layout.

At this regard, a theoretical formulation and implementation of a dynamic power control strategy on the RFID transmission front-end is provided. By adjusting the excitation amplitude of the RF carrier signal, the circuit modulates the power delivered to the RFID tag, allowing controlled interrogation and enabling the estimation of the reader-to-tag distance based on the analysis of backscattered signal strength and tag circuit activation power threshold. This approach allows not only identification of the tag, but also spatial inference from it, thus reinforcing the GNSS positional estimate with local proximity data. The RFID interface is therefore not merely an auxiliary component, but an active part of a closed-loop control system in which the GNSS configuration is locally adapted through low-power RF interactions. The proposed system is designed to operate with GNSS modules—such as the Zed-F9P from U-blox—that support external configuration, making the solution broadly applicable to existing platforms and fully customizable. The key element of the proposed integration of an RFID reader with a GNSS receiver relies in the possibility of reading useful information about field environment and data reliability from an additional observation point right from a tag, which serves as a sort of reference point: this would not be possible on non-differential GNSS receivers that do not allow real-time configuration adjustments and, furthermore, it allows the possibility of changing both the quality parameters related to satellite data that can be used or discarded plus configuring the working mode of the GNSS receiver itself. Finally, this paper presents the full design of the hybrid RFID–GNSS circuit, its hardware configuration, and its validation under realistic conditions typical of GNSS-degraded environments such as agricultural and forestry scenarios. The results confirm the idea that RFID-enhanced GNSS systems, when implemented at the circuit level, can achieve superior adaptability and robustness in complex environments, paving the way for low-power, autonomous, and reconfigurable navigation systems.

II. HYBRID GNSS-RFID CIRCUIT ARCHITECTURE

The architecture of the system aims to pass site-specific configuration data to a GNSS receiver by reading such information from RFID tags.

This is done as shown in Fig. 1, which shows how the MCU processes data and provides fine tuning in the form of thresholds that let the receiver adapt to the signal quality that is present in specific parts of an area. Several additional components, however, have been added for research purposes:

- Two additional ZED-F9P receivers were employed in order to provide benchmark at the same conditions without fine-tuning and for the same receiver under differential GNSS-RTK conditions, which serves as reference given the high degree of precision;
- Calibrated antennas have been employed, given the possibility of receiving satellite signals from L1 and L2 satellite bands with a peak gain of 5 dBi. These antennas also have a phase center error of ± 1 mm, 40 dB average low-noise amplifier (LNA) gain and maximum noise figure of 1.5 dB, representing a fairly good hardware to exploit the ZED-F9P capabilities;
- GPS, Glonass, Galileo and Beidou satellite constellations have been used to establish the position of the receivers, which let them achieve good signal stability after some minutes on cold start without using any previous data;
- The receiver is also able to perform first-order ionospheric delay cancellation, Doppler compensations and estimation of tropospheric and satellite-clock errors resulting in a reduced multipath effect on positioning accuracy.

Given the aforementioned hardware configuration, the standard GNSS receiver provides baseline position data while RTK-aided receiver is intended as reference for ground truth. The architecture is consequently meant to perform the following tasks:

- When a tag is detected, the system performs local reconfiguration of the RFID-aided GNSS receiver, adjusting parameters such as carrier-to-noise ratio (C/N0) thresholds, satellite's data angle-of-arrival (AoA) limits, and dimensional mode selection (2D/3D) in real-time: this is possible by sending configuration parameters through an U-Blox protocol to the GNSS receiver, which is consequently able to provide position solutions based on that setup instead of following a standard configuration.
- Configurations are then passed to the RFID-aided GNSS
- receiver module, which receives fine-tuned positioning adjustments derived from the tag context, leading to increased robustness and accuracy of the navigation solution given the possibility of avoid using noisy or multipath-affected data that have been previously assessed when georeferencing the tag by understanding, for instance, the minimum angle of arrival necessary to avoid effects generated by dense canopy;
- At a 5 Hz update frequency, all the three GNSS receivers generated a position solution while the MCU also passed, at the same frequency, RTCM corrections to the GNSS-RTK device. This has been done by using a 4G module to connect to NTRIP servers (Networked Transport of RTCM via Internet Protocol), which is essential to keep that differential receiver in ''fix'' mode indicating that it has solved all its uncertainties.

Additionally, the 4G module provides bidirectional communication capabilities, enabling remote diagnostics, and real-time control of the entire system from external operators or monitoring platforms. It should be mentioned that 4G, or any other mobile networks, are optional since they are not directly required to operate the circuit: they have been employed to receive corrections from an RTK base and to verify the device conditions as previously stated. As stated in the state of the art of mobile networks which can support GNSS, in addition, it is worth highlighting that exploiting 5G time-of-arrival capabilities [30] could be feasible in urban areas but should be used carefully in rural areas in order to avoid losing constant updates from NTRIP servers of RTCM correction sentences for GNSS-RTK systems.

The hybrid circuit architecture has been designed with a focus on modularity, compatibility, and operational autonomy. A major advantage lies in its support for generic hardware components conforming to open standards such as NMEA (National Marine Electronics Association) and RTCM, thereby avoiding dependence on proprietary protocols and maximizing interoperability with a wide range of commercial GNSS devices. Remote system supervision and reconfiguration are enabled through the 4G interface, which allows live monitoring of subsystem status, facilitates the injection of differential corrections, and supports operator intervention during mission-critical phases. This capability ensures high availability and responsiveness, even in dynamically changing environments. The architecture of the system adopts a ''setup-and-forget'' design philosophy. Once the RFID tag network has been deployed and the initial calibration is completed, the system requires minimal maintenance or manual recalibration, except in cases of substantial modifications to the physical layout or expansion of the tag infrastructure. This approach allows flexible data and configuration management, since in case of absence of RFID data the GNSS receiver would just stick to its own configuration, but any data that comes from tags would also reflect working conditions according to the field and adapt the receiver to the context. This power-control procedure is detailed in the next Section. In conclusion, the MCU orchestrates all data exchanges and subsystem interactions, producing refined GNSS solutions by merging standard satellite-based positioning with spatial inference derived from local RFID tag detections. This circuit-level fusion enables the system to dynamically adapt to the surrounding environment, providing context-aware configuration of the GNSS subsystem based on proximity to known georeferenced RFID anchors. The result is a closed-loop positioning system where GNSS parameters are tuned in real time via low-power RF interactions, significantly improving performance in GNSS-challenged environments.

III. CIRCUIT-LEVEL RFID-BASED POWER CONTROL METHOD FOR LOCALIZATION REFINEMENT: THEORETICAL ASPECTS

This section introduces a circuit-level localization refinement method for vehicles using a UHF RFID system, exploiting the interaction between fixed passive RFID tags and a mobile reader installed on the vehicle. This method assists the GNSS positioning system to improve overall precision. The reader transmitter is installed laterally, oriented to scan the fixed environment as the vehicle moves. The system iteratively adjusts the reader transmit power to determine the minimum

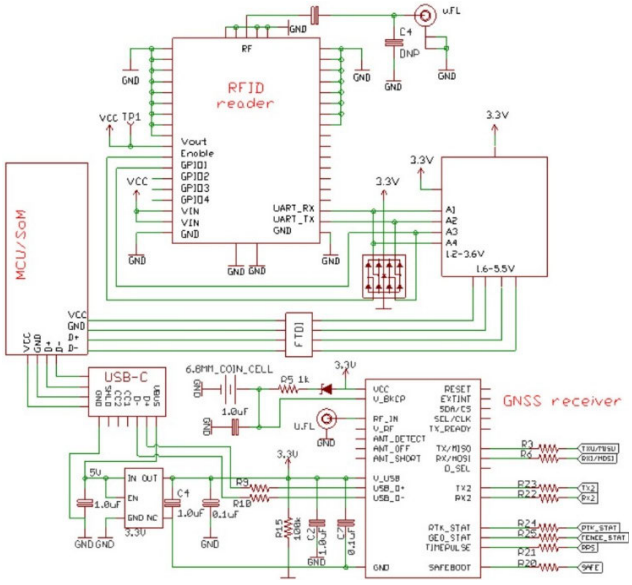

FIGURE 2. Hybrid RFID-GNSS circuit schematic.

level at which a tag can be successfully read, which serves as a proxy for estimating the distance between the reader and the tag and for correcting the GNSS information with local data.

The theoretical basis of the method stems from the RFID link budget model for the forward link [31], [32]. The received power at the tag is calculated as:

$$P_{Rx,tag} = P_{Tx} + G_{Tx} + G_{tag} - L_p(d) - \eta_{PLF}, \quad (1)$$

where P_{Tx} is the reader transmit power [dBm], G_{Tx} and G_{tag} are the antenna gains of the reader and tag respectively [dBi], $L_p(d)$ is the free-space path loss [dB] at distance d [m], η_{PLF} is the polarization loss factor between the reader and tag antenna. The path loss for UHF frequencies (e.g., $f = 868$ MHz) can be approximated as:

$$L_p(d) \approx 20 \cdot \log_{10}(d) + 58.81, \quad (2)$$

where the constant 58.81 dB results from $20 \cdot \log_{10}(f) - 147.55$ with $f = 866 \times 10^6$ Hz.

The tag is activated when the received power at the internal circuit equals its sensitivity value (i.e., $S_{IC} = -24dBm$).

The scanning procedure follows a bidirectional approach, as illustrated in Fig. 1. The reader begins with a transmit power P_{Tx} initialized at -*10 dBm* and incrementally increases it until the tag is successfully read (forward scan).

Once the tag is detected, the corresponding transmit power is denoted $P_{Tx.ON}$. Optionally, the reader performs a backward scan by decrementing the power from *30 dBm* downwards until the tag is no longer detected, yielding a value $P_{Tx.OFF}$.

The average value between these two points is:

$$P_{Tx,avg} = \left(P_{Tx,ON} + P_{Tx,off}\right)/2, \quad (3)$$

and it is used to estimate the distance as reported below:

$$d_{est} = 10^{\left((P_{Tx,avg} + G_{Tx} + G_{tag} - S_{IC} - \eta_{PLF} - 58.77)/20\right)}. \quad (4)$$

This bidirectional method enhances stability by mitigating asymmetries due to multipath and varying tag orientation. To accelerate the scanning process, a binary search (bisection) algorithm is adopted instead of linear stepwise adjustment. The initial power range is set between $P_{low} = -10dBm$ and $P_{high} = 30$ dBm. At each iteration, the midpoint power is calculated as:

$$P_{mid} = \left(P_{low} + P_{high}\right)/2. \quad (5)$$

The reader attempts to read the tag at P_{mid}. If the tag responds, P_{high} is updated to P_{mid}; otherwise, P_{low} is set to P_mid. The loop proceeds until the range $|P_{high} - P_{low}|$ falls below a defined threshold. The final midpoint is then used for distance estimation using the same link budget equation.

This hybrid scanning and estimation process enables fast and accurate localization refinement with minimal hardware overhead and no need for RSSI calibration. Fig. 3 shows the flowchart of the implemented algorithm where antenna gains are assumed to be $G_{Tx} = 6$ dBi and $G_{tag} = 2dBi$ respectively. The time cost of this scanning procedure has also been evaluated, since it may impact on the real-time applicability of the method. The bidirectional power scan requires multiple read attempts at different power levels until the threshold value is identified. The number of steps depends on the target resolution and the available power control granularity. For instance, with a resolution of 0.5 dB and an initial search range of 20 dB, the number of steps is about six (log2(20/0.5)). Considering a typical read rate of 100–150 successful tag responses per second and a reader settling time of a few milliseconds per power change, the overall duration of the scan is below 60 ms. In practical scenarios, even when tags move at moderate speeds (≈4–10 km/h in agricultural contexts and for industrial robots), they remain within the interrogation zone for a time interval that is much longer than the scan duration. This confirms that the proposed distance estimation procedure does not affect the real-time performance of the system. Similar analyses on fast-moving tags at railway speeds have been reported in [33] and [34], further supporting the feasibility of the method in our much slower application context.

IV. ELECTRICAL SCHEMATIC AND CIRCUIT IMPLEMENTATION

Fig. 2 illustrates the detailed electrical schematic of a hybrid RFID–GNSS circuit designed to enhance positioning performance in environments with obstructed or degraded satellite signals. The system integrates a UHF RFID reader and a GNSS receiver under the control of an MCU/SOM,

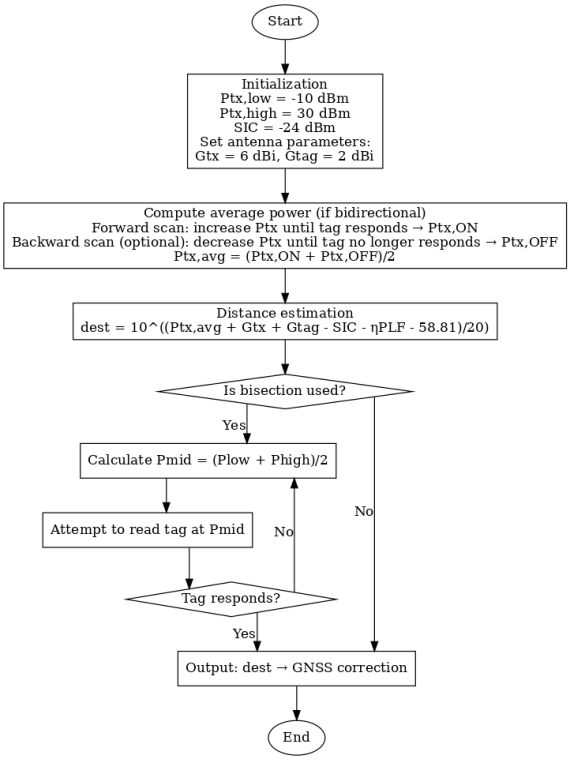

FIGURE 3. Circuit-level algorithm for RFID tag power scanning.

with power distribution and signal routing optimized for low-power embedded applications. All subsystems are powered by a regulated 3.3V supply generated from a 5V USB-C input via an integrated power management unit (PMU), which ensures stable voltage levels across the board. Bypass capacitors (0.1 μF and 1.0 μF) are placed in proximity to sensitive ICs to filter high-frequency noise and stabilize power delivery.

The RFID reader module is connected to the MCU through UART communication lines (UART_TX and UART_RX), enabling bi-directional data exchange. Its GPIO pins provide flexible digital I/O functionalities that can be configured by the MCU, while the Enable pin is used to selectively power the module on or off under software control. The RF front-end is routed through a *u.FL* connector to interface with an external UHF antenna, optimized for minimal signal loss and impedance matching. Notably, the RFID reader is not merely a passive listener but actively contributes to spatial inference. This is achieved by controlling the excitation power via the MCU and analyzing the backscattered signal from passive RFID tags, which are georeferenced and distributed in the environment. These tags not only identify specific locations but also support distance estimation, enabling local corrections to GNSS positioning: in GNSS-denied environments, or for cybersecurity anti-jamming purposes, reading a georeferenced tag means that the a vehicle can be located in a short range nearby the tag's position, working as an additional countermeasure of abnormal behavior of the GNSS receiver or against malicious attacks which is also becoming a new safety requirement in many countries, like Europe.

The GNSS receiver, also powered at 3.3V, is configured for dual-band or RTK operation and is equipped with an independent antenna line connected via a second u.FL connector. Communication with the MCU occurs through UART and optionally through an I^2C interface. Several control and status signals are exposed, such as EXTINT for timing synchronization, TIMEPULSE for fix monitoring, and TX_READY for data readiness. The module supports external configuration through standardized NMEA and RTCM protocols. A coin-cell battery provides backup voltage to maintain ephemeris data and RTC functionality, improving time-to-first-fix performance after temporary shutdowns. The MCU/SOM operates as the central logic controller, managing RFID interrogation sequences, GNSS reconfiguration commands, and interfacing with external communication systems. A dedicated USB interface supports firmware updates and serial debugging, with ESD protection implemented on the data lines. The 3.3V logic level throughout the system ensures compatibility and signal integrity across all modules.

From a circuit perspective, the design emphasizes modularity and robustness. The separation of analog, digital, and RF ground domains is supported by strategic grounding practices (evident from multiple GND points) to mitigate cross-domain interference. Signal lines are kept short and properly routed, particularly for RF traces connected to u.FL connectors. These considerations are crucial to maintain high-quality GNSS signal acquisition and accurate RFID tag detection in noisy environments.

FIGURE 4. Hybrid RFID-GNSS circuit physical implementation.

This circuit-level implementation exemplifies a closed-loop hybrid localization system where the GNSS receiver is dynamically reconfigured based on proximity interactions with RFID tags. The system supports real-time adjustments of GNSS parameters such as carrier-to-noise ratio thresholds and mode switching (2D/3D), which are adapted according to context-specific information embedded in RFID tags. The design is intended to be compatible with GNSS modules which support external command configuration via UART or I^2C.

In terms of functional features, the architecture is built on the use of generic components that rely on open communication standards like NMEA and RTCM, avoiding vendor-specific implementations. The inclusion of a 4G module (not shown in this circuit, but part of the full system architecture) enables remote telemetry and supports differential correction data via NTRIP, closing the loop with a cloud-based GNSS augmentation service. Moreover, the system is conceived with a ''setup-and-forget'' approach: once deployed and calibrated, the RFID network remains passive and maintenance-free, and any required update—such as layout changes or tag additions—only necessitates minimal reconfiguration. The RFID subsystem also supports dynamic control of transmission power and the ability to read, store, and overwrite tag data, making it a programmable and context-aware component of the positioning solution.

The physical prototype of the proposed hybrid RFID–GNSS system is shown in Fig. 4. To support the practical implementation, the system was realized using commercially available,

cost-efficient embedded platforms that meet the architectural requirements while ensuring scalability and ease of integration. For the main processing unit, a System on Module (SoM) based on the Raspberry Pi 5 was selected. This platform was chosen due to its high computational performance, versatile GPIO interface, and native UART connectivity, which enables seamless communication with both the RFID and GNSS subsystems. The Raspberry Pi was also equipped with a 4G communication HAT, which provides cellular connectivity for remote data exchange and facilitates the reception of differential corrections via the NTRIP protocol. The RFID subcircuit is built around the ThingMagic M6E Nano UHF RFID reader, which complies with EPCglobal Gen2 (ISO 18000-6C) standards and offers a compact, efficient solution for long-range tag interrogation. This module was interfaced with an Arduino UNO-compatible controller board used for development convenience and hardware-level abstraction, simplifying integration with the rest of the system. The RF front-end was connected to an external directional patch antenna through a u.FL port. The antenna, with dimensions of 223 mm $\times$ 220 mm $\times$ 60 mm and a gain of 6 dBi, provided robust interrogation performance while maintaining compact system geometry, suitable for mobile or outdoor deployment. For GNSS positioning, the u-blox ZED-F9P module was selected. This dual-frequency, high-precision GNSS receiver supports Real-Time Kinematic (RTK) positioning and exposes a broad range of configuration parameters accessible via UART and I^2C interfaces. The ZED-F9P's open protocol support (NMEA and RTCM) and ease of integration make it particularly suited for adaptive GNSS applications requiring external control and reconfiguration. Power to the entire system was supplied by a 10 Ah USB power bank, delivering 5V to the Raspberry Pi 5, which then redistributed regulated 3.3V and 5V power rails to the subsystems through its onboard PMU. This portable power configuration ensures autonomous operation in the field without the need for fixed infrastructure, supporting fully mobile deployments in GNSS-degraded environments.

V. CIRCUIT-LEVEL CONTROL MECHANISM

The circuit-level control mechanism of the hybrid RFID–GNSS system, illustrated in Fig. 5, forms the core of the architecture's adaptability and autonomy. This mechanism governs how data from UHF RFID tags is processed and used to influence GNSS receiver behavior in real time, based on the spatial context of the operating environment. The control logic of the system begins with the identification of a georeferenced RFID tag when it enters the read range of the antenna, typically between 0.5 and 2 meters. Once a tag is detected, the system performs a power check to evaluate the reliability of the signal and to evaluate its distance from the detected anchor tag. This involves adjusting the transmit power of the reader and comparing the strength of the received backscatter with the known excitation levels and the activation threshold of the tag. By verifying whether the tag responds consistently at reduced power levels, the microcontroller can estimate the relative distance and confirm that the detection is not the result of reflections or multipath propagation. This procedure acts as a spatial validity check to ensure that only short-range and direct interactions are considered reliable.

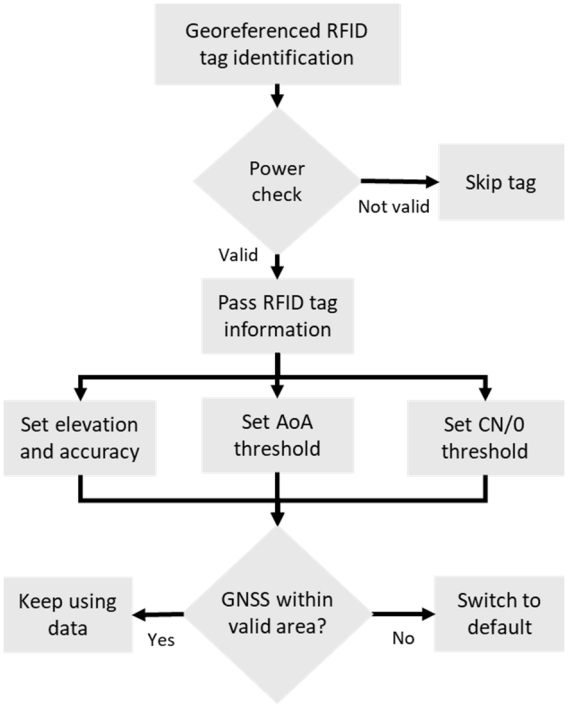

FIGURE 5. Hybrid RFID-GNSS circuit physical.

If the power check is passed, the microcontroller retrieves the data stored in the tag and determines whether it contains reconfiguration commands intended for the GNSS receiver. The content of the tag is then validated through multiple criteria, including the presence of a 2-byte CRC and a consistency check based on a validity radius field. Tags are disregarded if the estimated distance exceeds the specified validity radius. Only when all conditions are met, the microcontroller applies the configuration data to the receiver. This reconfiguration may involve adjusting key operating parameters such as the elevation mask, angle-of-arrival (AoA) threshold, and carrier-to-noise density ratio (CN0) threshold. These parameters are injected via UART into the GNSS receiver, such as the u-blox ZED-F9P, which supports external configuration through standard protocols. After applying the new settings, the system continuously monitors the GNSS solution to verify whether the device remains within the geofenced area associated with the detected tag. If the GNSS-derived position remains inside the tag's validity region, the parameters are retained. If the system moves outside this zone, it automatically resets the receiver to default configurations to prevent incorrect behavior due to outdated information. Not all tags are programmed to update all GNSS parameters; some may only override specific values based on local environmental needs—such as strong signal occlusion or increased mul-

tipath risk, which are assessed in the field when tags get georeferenced — while leaving other parameters unchanged if defaults already offer optimal performance. This selective and context-aware approach enables the RFID–GNSS hybrid system to dynamically adapt to complex environments without requiring constant user supervision.

TABLE 1. ZED-F9P Setting values, taken from U-BLOX interface description manual.

Parameter	Function	Unit	Value
UBX-CFG-NAV5	dynModel	0-10	Dynamic platform model, where 0 is portable, 2 is stationary, 3 is pedestrian, etc
	fixMode	1-3	Position fixing mode, 1 for 2D only, 2 for 3D only, 3 auto
	fixedAlt	m	Fixed altitude
	fixedAltVar	m^2	Fixed altitude variance
	minElev	deg	Minimum elevation for SV to be used
UBX-CFG-NAVX5	minSVs	#SVs	Minimum number of satellites to be used

Specifically, the block responsible for parsing and sending data to the GNSS receivers was performed through the open source pyubx2 library [35], that was able to interact with receivers through serial communication allowing the possibility of retrieving navigation data (NMEA GGA sentences, containing most of the useful information regarding position, accuracy and fix type) and of configuring the board through u-blox parameters (UBX) according to environmental and site conditions. Among the wide number of parameters that can be set this way (baud rate, reading frequency, navigation sentences to be shown in output, etc.) some of the most useful parameters for this research have been selected. A list of these parameters is hence reported in Tab. 1, indicating their unit of measurement and purpose.

The parameters that have been selected in table 1 were then measured in test fields to determine their optimal values. This way, a series of limit configurations has been determined as follows:

a. maximum altitude variability of 1 meter;
b. minimum of 5 degrees for angle of arrival (minimum elevation) in open sky conditions;
c. values between 20 and 30 degrees for angle of arrival in vineyards and roads;
d. a maximum of 45 degrees for angle of arrival in the most challenging conditions (path through woods);
e. Minimum acquisition thresholds for carrier to noise density ratio (CN0) set to 10 dBHz in most conditions, raised to 20 dBHz in open sky conditions to prevent the inclusion of extremely weak, multipath-dominated SV raw data while permitting the estimation of a position among the remaining satellites.

It is worth mentioning that the configurations presented in table 1 are just a part of a longer set of parameters that can be modified to improve the receiver's assessment (constellation selection, frequency of updates, etc.). This is simply limited by the size of data that the tag can store, or by the amount of space that users intend to leave for feedback purposes (with the circuit being able to write the tag).

The three receiver antennas were aligned along a line perpendicular to the direction of motion, but only the GNSS-RTK position could be considered reliable due to its low error rate: in order to estimate the error of the standard GNSS receiver and hybrid RFID-GNSS receiver, the real position of their antennas shall be estimated [36]. To do so, these steps are required:

- Identify the field vehicle's real path and estimate its bearing;
- For each coordinate in the path, estimate the corresponding coordinates of points belonging to the other two paths.

Hence, authors assumed the GNSS-RTK array of coordinates as reference path and computed the bearing among every two consequent points belonging to it. This calculation has been performed according to the formula:

$$\theta = arctan2\left(sin\left(\Delta\lambda\right) \cdot cos\left(\phi_2\right), cos\left(\phi_1\right) \cdot sin\left(\phi_2\right) + - sin\left(\phi_1\right) \cdot cos\left(\phi_2\right) \cdot cos\left(\Delta\lambda\right)\right), \quad (6)$$

where θ is the bearing, coordinates ϕ_1, λ_1 represent the latitude and longitude of the first of two consequent points and ϕ_2, λ_2 are the coordinates of the second one. Differences among λ coordinates are indicated as $\Delta\lambda = \lambda_2 - \lambda_1$. Knowing the bearing, it was possible to compute the coordinates of the two additional points that are positioned at a specific distance from the reference coordinate, which can be calculated as follows starting from their latitude:

$$\phi'_2 = arcsin(sin(\phi_1) \cdot cos(d/R) + cos(\phi_1) \cdot sin(d/R) \cdot cos(\theta)). \quad (7)$$

To determine ϕ'_2, the formula assumes R as the average radius of Earth (6371000m), $d$as the desired distance from the reference point (in this case, 35 and 70 cm which were the distances of RFID-aided GNSS and GNSS in standard conditions respectively), while θ is the bearing. Lastly, the longitude for each point can also be calculated as follows:

$$\lambda'_2 = \lambda_1 + arctan2\left(sin(\theta) \cdot sin(d/R) \cdot cos(\phi_1), cos(d/R) - sin(\phi_1) \cdot sin(\phi'_2)\right) \quad (8)$$

Repeating the calculation for all the coordinates in the GNSS-RTK paths provided two expected paths for each distance. The right path has been selected by graphical analysis

(a) (b) (c)

FIGURE 6. Hybrid RFID-GNSS test paths in agricultural and forestry contexts, representing a vineyard (a), a forest path (b), and a road near low-height trees and structures (c).

(a) (b) (c)

FIGURE 7. Details of the RFID-GNSS hardware setup. UHF RFID tags placed along the paths (a), the configuration of GNSS antennas on tractor's ROPS and RFID antenna on the left, (b) example of the operating conditions of the system in a vineyard (c).

from the KML file in which the coordinates have been merged into a linear string and checked in an interface for simplicity.

VI. CIRCUIT VALIDATION SCENARIOS AND EXPERIMENTAL VEHICLE CONFIGURATION

To validate the proposed hybrid RFID GNSS circuit and its on-hardware control mechanism, a series of field tests were conducted in environments characterized by degraded GNSS signal conditions. Specifically, three distinct agricultural and forestry scenarios were selected within the experimental farm of Tuscia University in Viterbo, Italy. These scenarios were chosen to induce GNSS performance variability through the presence of obstacles such as vineyard poles, trees of various heights, and structures, as well as areas with restricted sky visibility, which are known to cause multipath effects. RFID tags were strategically placed near these obstacles to trigger context-specific GNSS parameter adjustments. The three test routes, illustrated in Fig. 6, include a vineyard with multiple parallel rows (Fig. 6a), and a densely forested path (Fig. 6b), and a rural road flanked by cultivated fields and low vegetation (Fig. 6c). In the open-road scenario, RFID tags conveyed configurations with a carrier-to-noise density ratio (CN0) threshold set to 20 dBHz and satellite angle of arrival (AoA) limited to 20 degrees, effectively minimizing interference from low obstacles under open-sky conditions. In the vineyard, similar parameters were used, but AoA thresholds were raised to 30 degrees near taller vegetation, with some tags also enforcing a 2D-only mode through explicit elevation constraints. In the forested path, elevation constraints were omitted and AoA thresholds were increased to 45 degrees to compensate for tree canopy height. In all three cases, configuration validity was constrained by a geofencing mechanism based on rectangular zones defined by four georeferenced points, a format compatible with standard GNSS receiver requirements. The minimum tag-to-path distance was approximately 5 meters, particularly in the

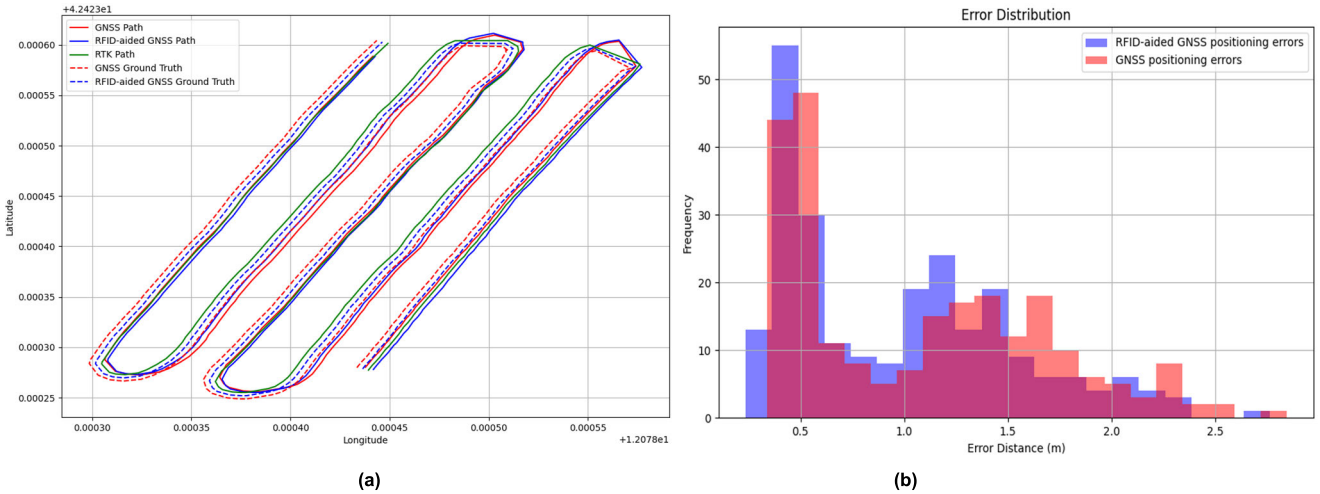

FIGURE 8. Circuit test in the vineyard: reconstructed test paths (a), and related positioning error distribution (b).

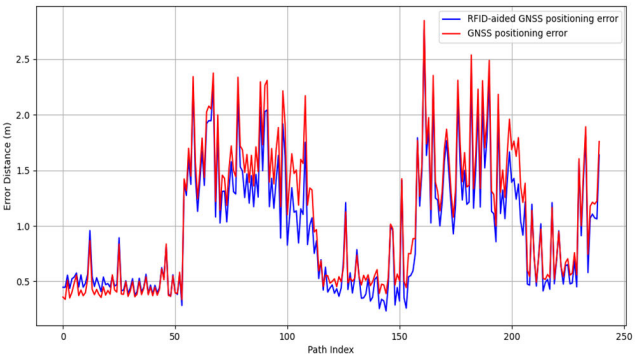

FIGURE 9. Absolute errors at each single point along the vineyard test path.

vineyard scenario, to ensure proper detection between rows. Fig. 7a shows the detail of an RFID Tag placed along the pathway.

To perform all the validation tests, the prototype of the hybrid RFID-GNSS circuit was placed on a field vehicle according to the setup presented in Fig. 7b and Fig. 7c. During a sunny day with clear sky, the GNSS readers were set to gather sufficient information to achieve a stable 3D position estimation and comparable horizontal accuracies, a process that usually takes some minutes if no previous data has been stored in battery-backed memory and that has been done by setting the receivers work at 5 Hz update frequency.

GNSS antennas were mounted on the vehicle roll-over protection structure (ROPS) using a T-slot bar, with a baseline separation of 35 centimeters, while the RFID antenna was installed on the right-hand side of the same structure. The main circuit prototype, as shown in Fig. 4, was secured behind the operator's seat without interfering with vehicle operation. The RFID reader antenna was configured to operate within a constrained range of 0.5 to 2 meters. This restriction was not due to hardware limitations but was intentionally introduced to ensure spatially selective and context-specific tag activation. In environments such as vineyards or forest paths, where tags may be located near repetitive structures, a limited read range helps prevent unintended configuration changes caused by the detection of tags positioned in adjacent rows or behind obstacles.

To further ensure that a detected tag is actually located within the desired proximity, the system implements a power modulation strategy. The reader dynamically adjusts its transmit power to determine the minimum level at which the tag can still be read reliably. This process enables verification that the detection is not caused by reflections or intermittent conditions. Only tags that are consistently read at a power level corresponding to the expected distance are considered valid. This mechanism guarantees that GNSS parameter reconfiguration occurs only when the vehicle is truly within the effective area associated with the tag.

If no tag is detected, or if the proximity verification fails, the GNSS receiver continues to operate with its default configuration, thus maintaining standard localization performance.

VII. RESULTS

This section presents the results of field validation tests conducted to evaluate the hybrid RFID GNSS circuit. The goal is to assess performance improvements in positioning accuracy under degraded signal conditions across three relevant use cases: vineyard operation, forest navigation, and open road driving. For each test path analysis, error distribution and absolute error along the path are provided. The path analysis shows the path generated by the receivers against the expected path according to the GNSS-RTK system, which has an error accuracy of 1 cm; error distributions and absolute errors along paths basically consent to compare the RFID-aided GNSS receiver to the same ZED-F9P receiver in standard working conditions.

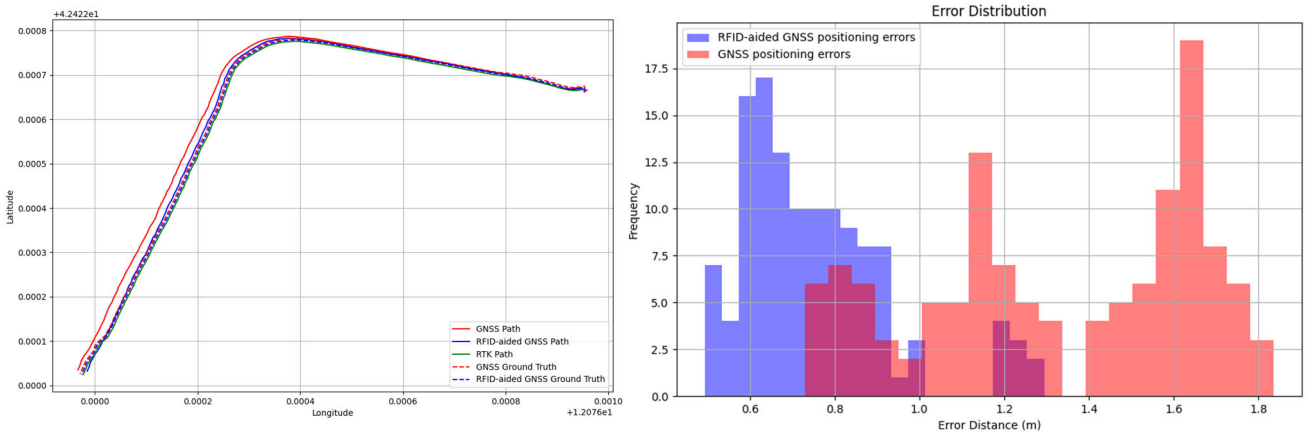

(a) (b)

FIGURE 10. Circuit test in the forest environment: reconstructed test paths (a), and related positioning error distribution (b).

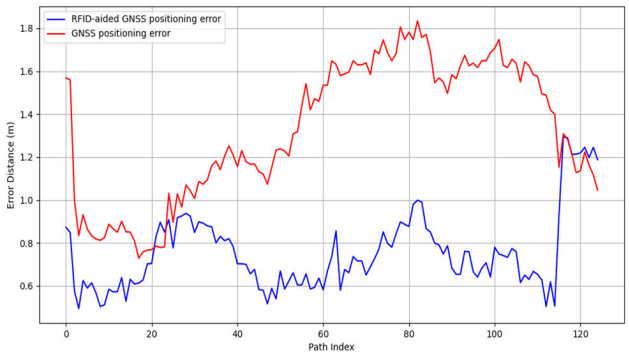

FIGURE 11. Absolute errors at each single point along the forest test path.

The vineyard test involved a standard agricultural operation with turning maneuvers at the end of each row. The compact dimensions of the field vehicle eliminated the need for additional maneuvers. Fig. 8a presents the expected path using dashed lines, while the paths from GNSS receivers are shown as solid lines of the same color; the reference GNSS RTK path is displayed in green. Starting from the bottom of the figure, the paths already exhibit variations, showing how positioning precision decreases as the field vehicle progresses toward the upper-right end of the vineyard. It is noteworthy that GNSS receivers may incorporate algorithms that assess the integrity of coordinates based on previous readings, resulting in different behaviors across the vineyard rows. The error distribution for this scenario, depicted in Fig. 8b, indicates a slight reduction in the frequency of larger errors for the RFID-aided GNSS receiver and an increased occurrence of smaller error distances, reflecting enhanced robustness. This becomes especially significant in environments where elevation impacts positioning. The median error values were 0.90 m for the RFID-aided receiver and 1.0 m for the standard receiver, with standard deviations of 0.54 m and 0.60 m, respectively. Additionally, absolute errors were evaluated along the entire route. As illustrated in Fig. 9, the improvement in error was consistent across the path, confirming the enhanced stability of the RFID-aided receiver.

In this scenario, the RFID tags also provided elevation, allowing all three configuration parameters (2D working mode, AoA, and CN0) to be supplied to the receiver. The RFID-aided receiver recorded a minimum error of 0.23 m and a maximum of 2.76 m, whereas the standard receiver ranged from 0.33 m to 2.84 m.

As second use-case, the forest path test was conducted in an area with dense vegetation and tall trees, incorporating a 45-degree AoA to compensate for limited open sky visibility. Fig. 10a illustrates a marked deviation of the standard GNSS receiver's path from the GNSS-RTK reference, while the RFID-aided receiver maintained consistent alignment with the expected path, suggesting better anticipated performance in both error distribution and absolute accuracy.

This is confirmed in Fig. 10b, where the RFID-aided receiver outperforms the standard setup, significantly enhancing vehicle positioning. Median errors were 0.70 m and 1.31 m for the RFID-aided and standard receivers, respectively, with standard deviations of 0.18 m and 0.32 m. Fig. 11 shows the absolute positioning error along the forest path, highlighting how error levels remained low at the start and end of the path—areas with reduced vegetation and fewer multipath effects.

As the vehicle entered the most obstructed zones, the standard receiver's performance declined, whereas the RFID-aided receiver maintained stable error levels, except for a minor degradation near the end due to turning and uneven terrain. The RFID-aided receiver recorded a minimum error of 0.49 m and a maximum of 1.29 m, compared to 0.72 m and 1.83 m for the standard receiver, which produced the highest observed error levels.

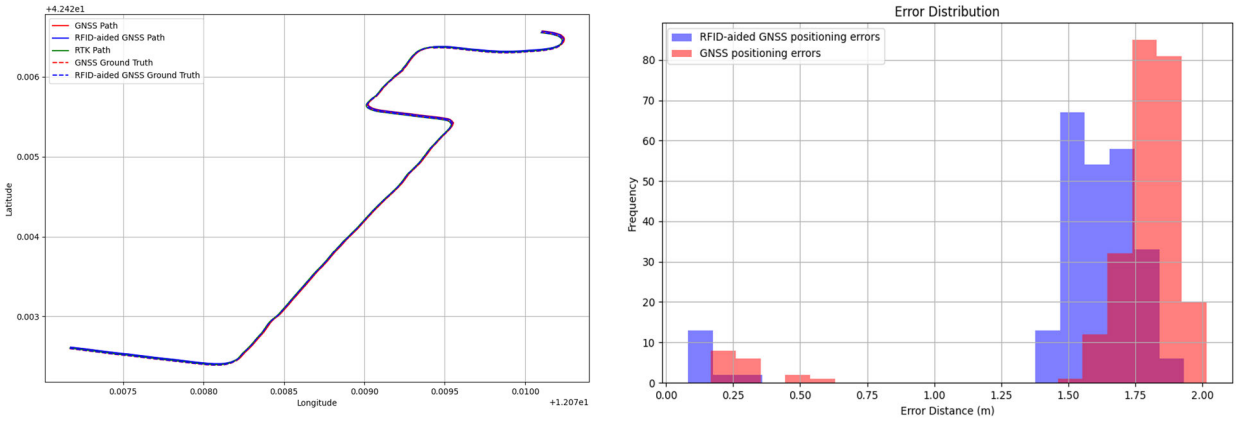

(a) (b)

FIGURE 12. Circuit test in the open road test scenario: reconstructed test paths (a), and related positioning error distribution (b).

Finally, the open-road test was initiated from the left side of the trajectory depicted in Fig. 6c, continuing along a straight segment followed by two turns, until the field vehicle eventually reached its storage area.

As clear from Fig. 12a, there the reconstructed trajectory is reported, no evident differences can be observed in the visualized paths between the RFID-aided and the standalone GNSS receivers, in this scenario. This is mainly due to the long distance covered and the inherently better GNSS conditions, characterized by minimal obstructions and continuous open-sky visibility. However, even under these favorable conditions, the analysis of positioning error distribution reveals a modest yet consistent improvement in localization accuracy when using the RFID-aided GNSS configuration. As shown in Fig. 12b, the error frequency profile indicates a slight shift toward lower error values, with the improvement observable across both small and large error magnitudes.

The absolute positioning error trend along the path, reported in Fig. 13, confirms a generally better performance of the RFID-aided receiver throughout the test. The configuration updates provided by the RFID tags placed along the road contributed to maintaining enhanced accuracy.

A significant reduction in positioning error is visible toward the end of the trajectory. Although this effect was also partially observed in the standalone GNSS receiver, it is believed to be influenced by external factors such as temporary improvements in satellite geometry or variations in the correction data received from the RTK base station—potentially due to a momentary switch between mountpoints in the regional base station network. For this scenario, the RFID-aided GNSS receiver exhibited a median positioning error of 1.62 m and a minimum and maximum error of 0.08 m and 1.93 m, respectively. In comparison, the standalone GNSS receiver had a median error of 1.80 m, with a minimum error of 0.16 m and a maximum of 2.01 m. In both cases, the standard deviation was 0.39 m, suggesting similar variability but a systematic benefit introduced by the RFID-based enhancements.

TABLE 2. Error comparison among RFID-Aided GNSS and standard GNSS receiver.

Test	Absolute mean difference	Relative mean difference
Vineyard	-0.1005 ± 0.01 m	9,39%
Open road	-0.1780 ± 0.01 m	10,43%
Woods	-0.5709 ± 0.01 m	43,08%

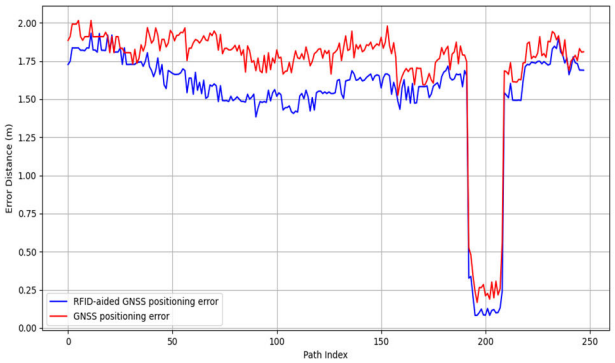

FIGURE 13. Absolute errors at each single point along the open road test path.

VIII. DISCUSSION

The experimental evaluation of the proposed hybrid RFID-GNSS circuit architecture confirms its effectiveness in enhancing positioning accuracy for vehicle navigation in signal-degraded environments. Unlike traditional GNSS receivers, the improved performance observed across all scenarios (vineyard, forest path, and open road) can be directly attributed to the dedicated circuit design, which integrates

UHF RFID functionality to enable adaptive reconfiguration of key GNSS receiver parameters. As summarized in Tab. 2, the hybrid circuit demonstrated superior accuracy in terms of mean and median errors as well as reduced error variance when compared to the standalone GNSS system.

These improvements stem not simply from the use of RFID as a concept, but from the implementation at circuit level of a dynamic control core, a high-frequency UHF front-end, and power management logic that enables fine-grained adjustment of GNSS operational modes based on the spatial presence of passive resonant RFID tags.

The most significant performance gain was observed in the forest scenario, where the dense canopy and low sky visibility severely limit GNSS reliability. In such contexts—well known for their multipath and obstruction-induced degradation—the circuit-enabled reconfiguration based on RFID tag proximity allowed the system to mitigate signal distortion and enhance localization robustness. This improvement is the result of the ability of the system to switch to a locally optimized configuration whenever the proximity of a tag is reliably confirmed. This condition is verified when the tag is detected at a distance between 0.5 and 2 meters, as validated by the power modulation algorithm. Only in this spatial range, the GNSS-related information encoded in the tag is considered reliable, including the recommended thresholds for satellite angle of arrival, carrier-to-noise ratio, altitude, and standard deviation of the altitude. The use of RFID tags enables spatially selective activation of the GNSS reconfiguration, which occurs only in zones where signal degradation is expected. This selective mechanism allows the application of more conservative receiver settings, such as higher CN0 thresholds, more restrictive elevation angle filters, or forced 2D positioning, applied only when the surrounding environment requires it. As a consequence, the system reduces the impact of multipath and obstruction-related distortions while maintaining nominal performance in open-sky conditions.

It is also worth noting that, when a tag is detected in conditions where trees obstruct or degrade a significant portion of the satellite signals arriving from the sides, the microcontroller temporarily increases the elevation mask and the acquisition threshold of the carrier-to-noise ratio. For example, the elevation mask is raised from 6 to 20 degrees and the C/N0 threshold from 10 dBHz to 25 dBHz, by issuing a UBX-CFG-NAV5 command within 120 ms from tag detection. This behavior explains the most significant improvement observed in the forested scenario, since the receiver will rely only on satellites with clear visibility and will exclude those obscured by vegetation.

Achieving sub-meter accuracy (0.7 m) in these conditions is comparable to float-mode RTK receivers, underscoring the value of a circuit-level sensor fusion strategy. Tests also confirmed that the low-cost receiver can achieve good results [37], [38], even when compared with RTK navigation methods. While prior literatures [2] and [39] has recognized the benefits of GNSS parameter tuning and sensor integration, this work demonstrates that these improvements are optimally leveraged when implemented in hardware via a dedicated hybrid circuit. The circuit's ability to adjust CN0 thresholds, elevation cutoffs, and mode switching logic through environmental cues stored in RFID tags allows for autonomous and context-aware tuning without reliance on external power or real-time network connectivity. In addition, the RFID subsystem offers a battery-less, low-maintenance infrastructure for encoding and delivering localized configuration data that can be further extended by increasing the number of tags based on field needs. The tags serve not only as spatial anchors, but also as passive transmitters of environmental context, enabling the circuit to infer and respond to metrics such as satellite visibility, vegetation density, or anticipated multipath.

The achieved level of position accuracy is significant due to the possibility of using the circuit as a low-cost and low-power GNSS positioning system, alternative to costly DGNSS/RTK systems for agricultural activities like spraying, tillage and yield mapping since such are often tasks that do not require centimetric precision in GNSS position accuracy. Interestingly, even in the open-road test—where sky visibility was nearly unobstructed—the hybrid circuit still provided measurable, albeit smaller, performance benefits. This suggests that the RFID-based tuning approach is not only effective in degraded environments but can provide marginal gains in nominal conditions, reinforcing its flexibility and scalability.

However, the system's performance is inherently tied to RFID tag detection range, which may limit deployment in large-scale applications unless denser tag distributions are adopted. Moreover, the necessity of georeferenced tag placement implies a preliminary setup phase, ideally suited for operational areas with repetitive activity (e.g., agricultural rows, forestry lanes, industrial yards).

Future research may investigate integrating longer-range RFID technologies, optimizing the circuit for ultra-low power operation, or enabling real-time parameter learning based on backscattered signal analysis. Furthermore, feedback from the RFID front-end could be used to trigger GNSS configuration changes based on dynamic indicators, such as humidity-induced signal loss or foliage density, processed directly by the circuit-level processing system. From a practical point of view, aiming instead at reaching a higher impact on real-life field tasks, the inclusion of AoA antennas might also allow to assess the relative position of machinery based on distance and signal's angle of arrival from multiple tags; another interesting feature, which would exploit the same circuit, could involve the use the same device to write both newer data or feedback on the tag (like achieved horizontal accuracy) and also any other kind of machinery information so that it also becomes a logbook for better tuning of upcoming vehicles or to store agricultural phytosanitary treatment data, which is a mandatory task in many countries, right on the tags placed in the field.

Finally, future research will be conducted to exploit the proposed hybrid RFID-GNSS circuit architecture in public parking facilities (indoor or outdoor), where autonomous robot-like mobile chargers can move visiting different parking spaces to charge electrical vehicles. Since installing a charging point at each parking space is an expensive way to increase the diffusion of electrical vehicles (particularly for indoor parking spaces), the idea underlying the project TER (Tools for Electric Recharging vehicle, grant MIMIT, CUP B89J25001580005) is to exploit autonomous robot-like mobile chargers, which decouple the vehicle charging requirement from parking space requirement. In order to achieve a precise autonomous navigation of the robot-like charger, which is requested to visit different parking spaces by moving among different parked electric vehicles, the idea is to exploit the proposed hybrid RFID-GNSS circuit architecture, where each RFID tag (placed at a proper point in the parking area) can effectively serve as a local anchor that can support fine-grained positioning refinement of the robot-like charger. The experimental evaluation of the proposed approach, in GNSS signal-degraded environments such as indoor parking spaces or outdoor parking spaces surrounded by buildings, will be investigated over the next few months within the TER project.

IX. CONCLUSION

In this work, a novel circuit-level hybrid RFID–GNSS architecture has been proposed to enhance positioning accuracy in signal-degraded environments such as forests, vineyards, and rural roads. The approach relies on the integration of passive UHF RFID tags acting as local anchors and a dedicated control circuit that dynamically adjusts GNSS receiver parameters in response to RFID-derived information. The circuit architecture of the system was fully developed, including schematic design and electrical configuration of its main functional blocks, such as the adaptive RFID excitation unit, the backscatter signal interface, and the embedded control logic responsible for distance estimation and GNSS reconfiguration. A physical prototype of the proposed circuit was designed, assembled, and integrated with a U-blox ZED-F9P GNSS module to experimentally validate its operation. The prototype supports dynamic control of GNSS parameters such as CN0 thresholds, satellite elevation filtering, and 2D/3D mode switching, based on the interaction with the RFID tag infrastructure. The overall system operates autonomously and without reliance on external corrections, making it particularly suitable for low-power and maintenance-free deployment in rural and remote contexts. The effectiveness of the system was assessed through real-world field tests in three representative signal-degraded scenarios. The hybrid RFID–GNSS circuit consistently outperformed the standalone GNSS receiver, with a measured positioning error reduction of up to 43.08% in dense forest conditions. Performance improvements were also confirmed in the vineyard and open-road scenarios. Additionally, the system demonstrated a notable decrease in positioning error variance, indicating improved stability and robustness. These findings confirm the viability of the developed circuit-level hybrid architecture as a compact, reconfigurable, and power-efficient solution for GNSS enhancement in challenging environments, paving the way for new classes of smart and autonomous navigation platforms.

ACKNOWLEDGMENT

The authors thank Dr. Riccardo Alemanno and Dr. Leonardo Assettati for their support with field setup and measurement campaigns.

REFERENCES

[1] R. F. Keefe, A. M. Wempe, R. M. Becker, E. G. Zimbelman, E. S. Nagler, S. L. Gilbert, and C. C. Caudill, "Positioning methods and the use of location and activity data in forests," *Forests*, vol. 10, no. 5, p. 458, May 2019, doi: 10.3390/f10050458.

[2] D. S. Chiu, G. MacGougan, D. S. Chiu, and G. MacGougan, "UWB assisted GPS RTK in hostile environments," in *Proc. Inst. Navigat., Nat. Tech. Meeting*, 2008, pp. 532–542. [Online]. Available: https://www.scopus.com/inward/record.uri?eid=2-s2.0-57649210806&partnerID=40&md5=cb2841e05301b264a73f3a1744a623ce

[3] G. Retscher, D. Kiss, and J. Gabela, "Fusion of GNSS pseudo-ranges with UWB ranges based on clustering and weighted least squares," *Sensors*, vol. 23, no. 6, p. 3303, Mar. 2023, doi: 10.3390/s23063303.

[4] K. Chawla, C. McFarland, G. Robins, and C. Shope, "Real-time RFID localization using RSS," in *Proc. Int. Conf. Localization GNSS (ICL-GNSS)*, Jun. 2013, pp. 1–6, doi: 10.1109/ICL-GNSS.2013.6577259.

[5] D. Monarca, P. Rossi, R. Alemanno, F. Cossio, P. Nepa, A. Motroni, R. Gabbrielli, M. Pirozzi, C. Console, and M. Cecchini, "Autonomous vehicles management in agriculture with Bluetooth low energy (BLE) and passive radio frequency identification (RFID) for obstacle avoidance," *Sustainability*, vol. 14, no. 15, p. 9393, Aug. 2022, doi: 10.3390/su14159393.

[6] L. Catarinucci, G. Cecchi, F. P. Chietera, M. Cecchini, R. Colella, R. Gabbrielli, L. Landi, L. Marrazzini, D. Monarca, T. Montanaro, A. Motroni, P. Nepa, L. Patrono, M. Pirozzi, D. Puri, P. Rossi, I. Sergi, E. Tavanti, and L. Vita, "Enhancing worker safety in unmanned agricultural environments through the integration of RFID, RTK, UWB, and LIDAR: Insights from research projects," in *Proc. 8th Int. Conf. Smart Sustain. Technol. (SpliTech)*, Jun. 2023, pp. 1–6, doi: 10.23919/splitech58164.2023.10193236.

[7] H.-Y. Yu and J.-J. Chen, "An intelligent space location identification system based on passive RFID tags," in *Proc.-Int. Conf. Mach. Learn. Cybern.*, Jun. 2014, pp. 428–433, doi: 10.1109/ICMLC.2014.7009153.

[8] L. Landi, A. Buffi, M. Marracci, A. Stecconi, P. D. Leone, F. Bernardini, and L. Didonato, "Localization systems for safety applications in industrial scenarios," in *Proc. 31st Eur. Saf. Rel. Conf. (ESREL)*, 2021, pp. 2413–2419, doi: 10.3850/978-981-18-2016-8_261-cd.

[9] Y. Zhang, R. Wang, and Z. Xing, "Collaborative navigation in urban environments via GNSS and 5G signals," in *Proc. IEEE Int. Conf. Commun.*, May 2023, pp. 6275–6280, doi: 10.1109/ICC45041.2023.10279482.

[10] Y. Zhang, R. Wang, and Z. Xing, "A robust evolutionary particle filter technique for integrated navigation in urban environments via GNSS and 5G signals," *IEEE Trans. Ind. Informat.*, vol. 20, no. 4, pp. 6866–6878, Apr. 2024, doi: 10.1109/TII.2024.3353849.

[11] C. Jing, S. Wang, M. Wang, M. Du, L. Zhou, T. Sun, and J. Wang, "A low-cost collaborative location scheme with GNSS and RFID for the Internet of Things," *ISPRS Int. J. Geo-Inf.*, vol. 7, no. 5, p. 180, May 2018, doi: 10.3390/ijgi7050180.

[12] M. Du, C. Jing, and M. Du, "Tag location method integrating GNSS and RFID technology," *J. Global Positioning Syst.*, vol. 14, no. 1, pp. 1–16, Dec. 2016, doi: 10.1186/s41445-016-0002-8.

[13] T.-K. Dao, H.-L. Nguyen, T.-T. Pham, E. Castelli, V.-T. Nguyen, and D.-V. Nguyen, "User localization in complex environments by multimodal combination of GPS, WiFi, RFID, and pedometer technologies," *Sci. World J.*, vol. 2014, pp. 1–7, Sep. 2014, doi: 10.1155/2014/814538.

[14] M. Khosyi'in, S. A. D. Prasetyowati, Z. Nawawi, and B. Y. Suprapto, "Review and design of GPS-RFID localization for autonomous vehicle navigation," in *Proc. 2nd Int. Conf. Electron. Electr. Eng. Technol.*, New York, NY, USA, Sep. 2019, pp. 42–46, doi: 10.1145/3362752.3362766.
[15] Y. G. Ampatzidis, S. G. Vougioukas, D. D. Bochtis, and C. A. Tsatsarelis, "A yield mapping system for hand-harvested fruits based on RFID and GPS location technologies: Field testing," *Precis. Agricult.*, vol. 10, no. 1, pp. 63–72, Feb. 2009, doi: 10.1007/s11119-008-9095-8.
[16] A. Ascher, M. Eberhardt, M. Lehner, B. Lippert, and E. Biebl, "A small UHF-RFID transponder with integrated GPS for localization applications," in *Proc. Int. EURASIP Workshop RFID Technol. (EURFID)*, Oct. 2015, pp. 132–139, doi: 10.1109/EURFID.2015.7332398.
[17] C. Zhai, A. Landers, and B. Zhang, "An RFID-based solution for monitoring sprayer movement in an orchard/vineyard," *Precis. Agricult.*, vol. 19, no. 3, pp. 477–496, Jun. 2018, doi: 10.1007/s11119-017-9531-8.
[18] R. Chen, X. Huang, Y. Zhou, Y. Hui, and N. Cheng, "UHF-RFID-Based real-time vehicle localization in GPS-less environments," *IEEE Trans. Intell. Transp. Syst.*, vol. 23, no. 7, pp. 9286–9293, Jul. 2022, doi: 10.1109/TITS.2021.3085824.
[19] C. Bajaj, D. K. Upadhyay, S. Kumar, and B. K. Kanaujia, "GPS-integrated RFID antenna with AMC backing for IoT-based sensing and tracking applications," *IEEE Trans. Antennas Propag.*, vol. 72, no. 2, pp. 1929–1934, Feb. 2024, doi: 10.1109/TAP.2023.3332481.
[20] W. He, E. L. Tan, E. W. Lee, and T. Y. Li, "A solution for integrated track and trace in supply chain based on RFID & GPS," in *Proc. IEEE Conf. Emerg. Technol. Factory Autom.*, Sep. 2009, pp. 1–6, doi: 10.1109/ETFA.2009.5347146.
[21] Q. Fu and G. Retscher, "Active RFID trilateration and location fingerprinting based on RSSI for pedestrian navigation," *J. Navigat.*, vol. 62, no. 2, pp. 323–340, Apr. 2009, doi: 10.1017/s0373463308005195.
[22] Q. Liu, W. Li, S. Zhang, Y. Nan, J. Peng, and Z. Ma, "Analysis of signal-to-noise ratio retrieved from multi-GNSS satellite data of land surface reflections," *GPS Solutions*, vol. 27, no. 3, pp. 1–12, Jul. 2023, doi: 10.1007/s10291-023-01502-9.
[23] T. Brun, Z. Xu, I. Petrunin, R. Wong, and R. Grech, "Machine learning enhanced signal quality assessment leveraged with GDOP for GNSS/INS fusion," in *Proc. IEEE Int. Instrum. Meas. Technol. Conf. (I2MTC)*, May 2024, pp. 1–6, doi: 10.1109/I2MTC60896.2024.10560699.
[24] S. Xia, S. Jin, and X. Jin, "Estimation and evaluation of zenith tropospheric delay from single and multiple GNSS observations," *Remote Sens.*, vol. 15, no. 23, p. 5457, Nov. 2023, doi: 10.3390/rs15235457.
[25] V. Hamza, B. Stopar, O. Sterle, and P. Pavlovčič-Prešeren, "Low-cost dual-frequency GNSS receivers and antennas for surveying in urban areas," *Sensors*, vol. 23, no. 5, p. 2861, Mar. 2023, doi: 10.3390/s23052861.
[26] *U-Blox ZED-F9P GNSS Receiver*. Accessed: Jan. 19, 2025. [Online]. Available: https://www.u-blox.com/en/product/zed-f9p-module
[27] O. Abdi, J. Uusitalo, J. Pietarinen, and A. Lajunen, "Evaluation of forest features determining GNSS positioning accuracy of a novel low-cost, mobile RTK system using LiDAR and TreeNet," *Remote Sens.*, vol. 14, no. 12, p. 2856, Jun. 2022, doi: 10.3390/rs14122856.
[28] R. Hohensinn, R. Stauffer, M. F. Glaner, I. D. Herrera Pinzón, E. Vuadens, Y. Rossi, J. Clinton, and M. Rothacher, "Low-cost GNSS and real-time PPP: Assessing the precision of the u-blox ZED-F9P for kinematic monitoring applications," *Remote Sens.*, vol. 14, no. 20, p. 5100, Oct. 2022, doi: 10.3390/rs14205100.
[29] U. Robustelli, M. Cutugno, and G. Pugliano, "Low-cost GNSS and PPP-RTK: Investigating the capabilities of the u-blox ZED-F9P module," *Sensors*, vol. 23, no. 13, p. 6074, Jul. 2023, doi: 10.3390/s23136074.
[30] Y. Zhang, R. Wang, and E. Liu, "Cooperative UAVs placement optimization for best multistatic time-of-arrival localization in 5G networks," *IEEE Trans. Wireless Commun.*, vol. 24, no. 4, pp. 3561–3574, Apr. 2025, doi: 10.1109/TWC.2025.3532411.
[31] R. Colella, L. Catarinucci, P. Coppola, and L. Tarricone, "Measurement platform for electromagnetic characterization and performance evaluation of UHF RFID tags," *IEEE Trans. Instrum. Meas.*, vol. 65, no. 4, pp. 905–914, Apr. 2016, doi: 10.1109/TIM.2016.2516322.
[32] D. A. Loku Galappaththige, F. Rezaei, C. Tellambura, and S. Herath, "Link budget analysis for backscatter-based passive IoT," *IEEE Access*, vol. 10, pp. 128890–128922, 2022, doi: 10.1109/ACCESS.2022.3227499.
[33] B.-K. Cho, "RFID antenna for position detection of train," in *Future Information Technology*. Berlin, Germany: Springer, 2014, pp. 903–908.
[34] X. Zhang, V. Lakafosis, A. Traille, and M. M. Tentzeris, "Performance analysis of 'fast-moving' RFID tags in state-of-the-art high-speed railway systems," in *Proc. IEEE Int. Conf. RFID-Technol. Appl.*, Jun. 2010, pp. 281–285, doi: 10.1109/RFID-TA.2010.5529918.
[35] *Pyubx2–Python Package*. Accessed: Jan. 19, 2025. [Online]. Available: https://github.com/semuconsulting/pyubx2
[36] T. Vincenty, "Direct and inverse solutions of geodesics on the ellipsoid with application of nested equations," *Surv. Rev.*, vol. 23, no. 176, pp. 88–93, Apr. 1975, doi: 10.1179/sre.1975.23.176.88.
[37] S. Öğütcü, S. Alçay, H. Duman, B. N. Özdemir, and Ü. Koray, "Data integrity and quality analysis of low cost zed-f9p u-blox gnss receiver," *Konya J. Eng. Sci.*, vol. 2023, pp. 660–667, May 2023, doi: 10.36306/konjes.1268932.
[38] D. Janos, P. Kuras, and L. Ortyl, "Evaluation of low-cost RTK GNSS receiver in motion under demanding conditions," *Measurement*, vol. 201, Sep. 2022, Art. no. 111647, doi: 10.1016/j.measurement.2022.111647.
[39] D. Amalfitano, M. Cutugno, U. Robustelli, and G. Pugliano, "Designing and testing an IoT low-cost PPP-RTK augmented GNSS location device," *Sensors*, vol. 24, no. 2, p. 646, Jan. 2024, doi: 10.3390/s24020646.

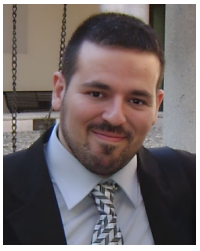

PIERLUIGI ROSSI (Member, IEEE) received the master's degree in safety engineering from Sapienza University, Rome, Italy, and the Ph.D. degree in engineering for energy and the environment from Tuscia University, Viterbo, Italy, with a thesis on digital-based solutions and algorithms for competitive safety in agricultural environments. He is currently a Research Associate with the Department of Agriculture and Forest Sciences, Tuscia University. He has conducted studies on the implementation of low-cost and low-power wireless solutions for agricultural machinery, focusing on fleet management systems, GNSS, and the Internet of Things (IoT) devices for machinery and workers' localization. Among his key works, he has co-authored studies on tractor performance analyses in vineyard activities and autonomous vehicle management involving the use of BLE, Lidar, GNSS-RTK, and RFID for obstacle avoidance purposes. He is also involved in the coordination and deployment of national projects funded by the Italian's National Institute for Insurance against Accidents at Work (INAIL) as a participant in the project called "Smart system for operator safety management in work environments with remotely operated mobile machinery" (SMARTGRID), in 2019, as a Co-Project Leader for "System for Detection and Tracking of Fixed and Moving Obstacles for Agricultural Self-Propelled Machines" (SIRTRAck), in 2022, Compact Tractor 4.0, in 2022, and lastly as a work-package leader for the project "Machine 5.0," in 2024.

LUCA CATARINUCCI (Senior Member, IEEE) is currently a Professor of electromagnetic fields with the Department of Innovation Engineering, University of Salento, Italy, and holds the chairs of ''Microwaves'' and ''Electromagnetic Solutions for Hi-Tech.'' He leads a dynamic Research Group with a keen focus on RFID and cutting-edge electromagnetic technologies in the realm of IoT. His research also encompasses the deployment of advanced electromagnetic simulation tools, the electromagnetic characterization of diverse materials, and the application of time-domain reflectometry for the qualitative and quantitative assessment of fluids. A significant part of his current research is deeply rooted in RFID-related pursuits, spanning across a broad spectrum including antenna and system design, the seamless integration of sensors and RFID tags, innovative strategies for RFID-based robot navigation, and pioneering methods for tag characterization, optimization, and design. His collaborations extend to numerous research teams, delving into areas, such as antenna arrays, the manufacturing of antennas, and the role of 3D-printing in electromagnetics, among others. Throughout his career, he has been the scientific lead on multiple national and European research projects and technology transfer projects in the fields of electromagnetics, RFID, and smart wireless technologies. He has authored more than 200 papers in international journals and conferences, and four chapters in internationally recognized books. He is also the co-inventor of two national patents. In his professional journey, he is the Chair of the IEEE Technical Committee on Additively Manufactured Electronic Systems. He held the position of Vice President of Technical Activities at the IEEE Council on RFID (CRFID), from 2022 to 2023. As of now, he is the President-Elect of the IEEE Council on RFID for the two-year term, from 2024 to 2025.

MASSIMO CECCHINI (Senior Member, IEEE) is currently a Full Professor with the Department of Agricultural and Forest Sciences, Tuscia University, Italy. He is the Head of the Laboratory of Ergonomics and Work Safety and serves as the President of the Master's Degree Course, Digital Management of Agriculture and Mountain Areas. He is a member of the Steering Committee for the recent editions of the International Conference Ragusa SHWA–Safety, Health, and Welfare in Agro-Food Systems, and he is also the Former President of the 5th Section (Ergonomics) of the Italian Society of Agricultural Engineering (AIIA) and a corresponding member of the Italian Accademia dei Georgofili. He is the author of more than 350 scientific articles on safety in agriculture, and has been organizing the Safety Day study day at Tuscia University for 14 years, in conjunction with the European Week for Safety and Health at Work. His research focuses on the field of agricultural engineering and is the project leader of the ''Compact Tractor 4.0'' project, funded by the Italian's National Institute for Insurance Against Accidents at Work (INAIL) and focusing on the development of a low-profile hybrid or electric propulsion tractor capable of supporting industry 4.0 technologies and equipped with a fixed rollover protective structure (ROPS).

GIUSEPPE GRASSI (Senior Member, IEEE) received the Laurea degree (Hons.) in electronic engineering from Università di Bari, Bari, Italy, and the Ph.D. degree in electrical engineering from the Politecnico di Bari, Bari, in 1994. In 1994, he joined the Dipartimento di Ingegneria dell'Innovazione, University of Salento, Lecce, Italy, where he is currently a Professor of electrical engineering. He has published more than 180 articles in international journals (source: Web of Science) and more than 110 papers in proceedings of international/national conferences. His research interests include complex systems, circuit theory and design, chaotic and hyperchaotic circuits, artificial intelligence, neural networks theory and applications, circuits, and systems for RFID applications. He is a member of the IEEE Technical Committee on Nonlinear Circuits and Systems. From January 2012 to January 2016, he served as the Director of the Centro Cultura Innovativa d'Impresa, the Interdepartmental Center of the University of Salento with an annual budget of more than ten million euros in research on emerging technologies. From January 2016 to January 2019, he served as the Head of the Department of Engineering for Innovation, University of Salento. Since November 2019, he has served as a Pro-Vice Chancellor for Administration and Finance. From 2004 to 2007, he was an Associate Editor for the Dynamics of Impulsive Continuous and Discrete Time Systems-Series B. From 2008 to 2011, he served as an Associate Editor for IEEE TRANSACTIONS ON CIRCUITS AND SYSTEMS—II: EXPRESS BRIEFS. From 2010 to 2013, he served as an Associate Editor for *IEEE CAS Magazine*.

RICCARDO COLELLA (Senior Member, IEEE) received the master's degree (Hons.) in telecommunications engineering and the Ph.D. degree in information engineering from the University of Salento, Lecce, Italy, in 2010 and 2015, respectively. He is currently an Assistant Professor of electrical engineering with the University of Salento. He has authored about 160 articles, contributed two book chapters, and holds one patent. His research interests include nonlinear neuromorphic circuits and memristors for intelligent high-frequency and backscattering applications. His activity covers modeling and design of circuits for passive RFID sensing, RF-dc energy conversion, power network monitoring, and characterization of materials for 3D-printable electronics. He serves as the Vice President for Member Services of the IEEE Council on Radio-Frequency Identification and is a member of the Sensory Systems Technical Committee of the IEEE Circuits and Systems Society (CASS). He has received the International URSI Young Scientist Award, the IEEE MTT-S C&S Italy Award, and the ''Giorgio Barzilai'' Scientific Award. He is an Associate Editor of IEEE OPEN JOURNAL OF CIRCUITS AND SYSTEMS (OJ-CAS) and IEEE JOURNAL OF RADIO FREQUENCY IDENTIFICATION (JRFID).